# Solvent Induced Proton Polarization within the Nuclear-Electronic Orbital Framework

Eleftherios Lambros,[†] Benjamin Link,[†] Mathew Chow,[‡] Sharon Hammes-Schiffer,[*,‡] and Xiaosong Li[*,†]

[†]*Department of Chemistry, University of Washington, Seattle, WA, 98195*

[‡]*Department of Chemistry, Yale University, New Haven, CT 06520, USA*

E-mail: sharon.hammes-schiffer@yale.edu; xsli@uw.edu

May 6, 2023

**Abstract**

To explicitly account for nuclear quantum effects and solvent environments in simulations of chemical processes, the nuclear-electronic orbital approach is coupled with a polarizable continuum model (PCM). This NEO-PCM approach is used to explore the influence of solvation on nuclear polarization through applications to a water dimer and a set of protonated water tetramers. Nuclear polarization in these species is analyzed in terms of changes in proton density and oxygen-hydrogen bond length. Solvation is shown to enhance nuclear polarization with increasing dielectric constant. For the water dimer, the internal, hydrogen-bonded proton is shown to polarize more than the external, free proton. Moreover, proton quantization leads to greater solvent polarization through their mutual polarization. These calculations highlight the complex interplay among electronic, nuclear, and solvent polarization in chemical systems.

# TOC Graphic

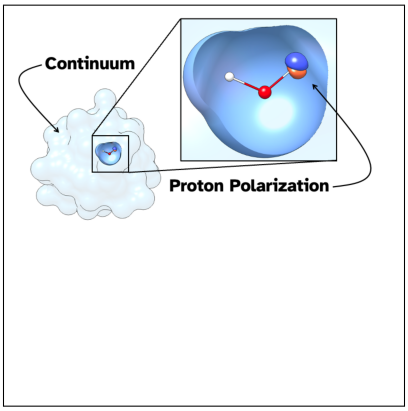

Many biological and chemical processes inherently rely on nuclear quantum effects, including hydrogen tunneling, zero-point energy (ZPE), and vibrational excited states. For nonadiabatic processes such as proton-coupled electron transfer or excited-state intramolecular proton transfer, which often occur in solution, an explicit treatment of nuclear quantum effects is necessary to account for these important energetic and dynamical contributions.[1–3] In general, the description of nuclear quantum effects depends on the form of the nuclear wave function and its coupling to the electronic subsystem. In the context of solution-phase processes, it is necessary to understand how the nuclear wave function and associated density react to various solvent environments and, furthermore, how nuclear-electronic correlation is modulated by environmental effects.

In terms of formalism, the nuclear-electronic orbital (NEO) framework[4] is attractive because it represents the nuclear subsystem on the same quantum mechanical footing as the electronic subsystem, avoiding the Born-Oppenheimer separation between the electrons and select nuclei. In this approach, electronic and nuclear degrees of freedom can be treated fully variationally according to the time-dependent or time-independent Schrödinger equation. The NEO approach can be used to study many processes for which a multicomponent description of the system is necessary to account for nuclear quantum effects on the energetic, vibronic, and dynamical properties of the system. This approach is particularly useful for proton transfer reactions, which can occur in the nonadiabatic regime, such as in proton-coupled electron transfer or excited-state intramolecular proton transfer. To address these challenges, the NEO approach has been extended to allow for real time (RT) propagation of protons and electrons in both pure RT-NEO,[5] as well as within semiclassical NEO-Ehrenfest dynamics.[6–8] Beyond density functional theory (DFT) and Hartree-Fock (HF) theory,[4,9–11] the NEO approach has also been adapted to more generalized wave function methods such as NEO-coupled cluster[12] and second-order perturbation theory.[2,13]

To incorporate solvation effects, the NEO approach[14] and related multicomponent methods[15,16] have been combined with a polarizable continuum model (PCM).[17–25] Briefly, the

PCM formalism describes solvent environments by embedding the molecule in a cavity immersed in a dielectric continuum with inertial and static dielectric constants corresponding to the specified solvent. The interaction between the molecule and the solvent is described by the reaction field formalism, which includes feedback between the molecule and the solvent environment. In this formalism, the solvation free energy is obtained as the electrostatic interaction between the electronic density of the molecule and the cavity potential, which represents the solvent polarization response as a set of discretized apparent surface charges (ASCs) on the cavity.

Various PCM schemes have been formulated and have been widely used in computational studies of biomolecular chemistry and chemical reactions in solvent environments, as well as for nonequilibrium processes such as excited state dynamics in solution.[18,19] The differences between these PCM techniques arise mainly from the method used to initialize the boundary conditions for the Poisson problem and the corresponding solution method. For example, conductor-like models such as C-PCM,[26,27] COSMO,[28] and ddCOSMO[29–31] rely on the vanishing potential property on the cavity surface, whereas proper PCM approaches, including integral equation formalism PCM (IEF-PCM)[32–34] and SS(V)PE-PCM,[35,36] are set up from the normal component of the dielectric boundary conditions.[18,19] It has also been shown that the generalized Born (GB) solvation model becomes formally equivalent to C-PCM under certain conditions in the conductor limit.[37,38] It is important to emphasize here that all PCM schemes describe the solvent as a continuum. A significant advantage of these schemes is that they implicitly integrate over the solvent degrees of freedom, and thus the solvation energies obtained from such calculations are formally free energies. However, these schemes cannot explicitly describe important effects such as hydrogen bonding between solute and solvent molecules, where an atomistic description of the environment is needed.

Herein, we characterize the response of the nuclear density to solvent environments using the NEO-IEF-PCM approach. Although the response of the electronic density to continuum solvent environments has been explored with conventional electronic structure PCM

methods, for instance, in the context of the outlying charge problem[39] and nonequilibrum solvation,[27,40] the nuclear density response has not been investigated previously within the NEO framework. By treating one or all protons quantum mechanically on the same level as the electrons, we are able to compute the proton polarization, defined as the change in the proton density, due to solvation. In addition, we are able to compute the impact of proton quantization on the solvent polarization, measured in terms of the apparent surface charges. These analyses provide a deep understanding of the mutual polarization between quantized nuclei and the surrounding solvent environment.

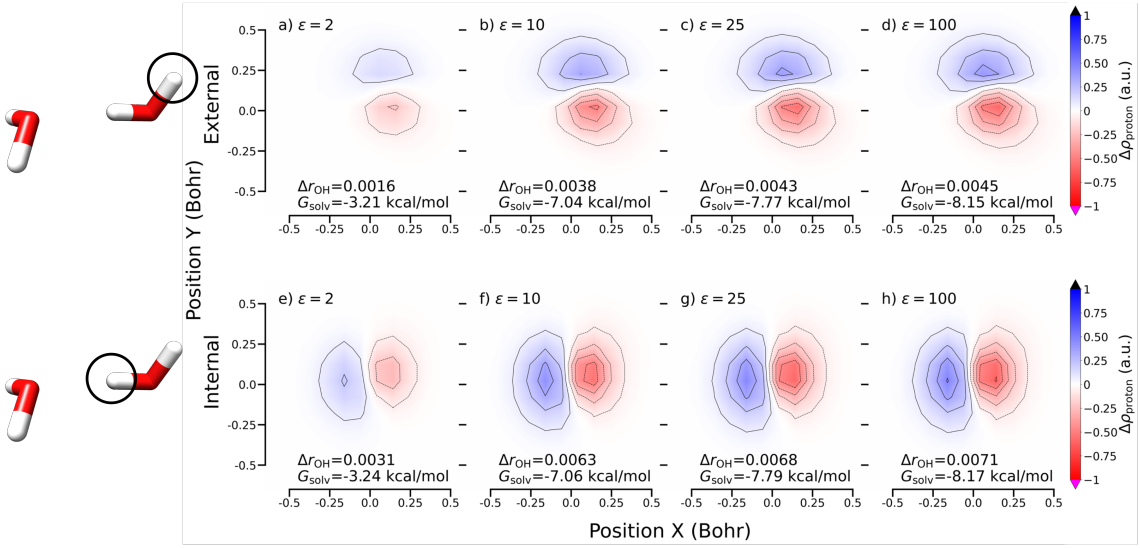


**Figure 1.** Polarization of the proton density in a water dimer upon solvation, where the proton polarization is defined as the proton density difference between solvent and vacuum (see Eq. (2)). The proton densities were computed with NEO-PCM for a quantum mechanical treatment of **a-d)** the external hydrogen and **e-h)** the internal hydrogen as a function of dielectric constant from $\varepsilon = 2 - 100$. Changes in bond lengths are shown in Bohr, and solvation free energies are given as $G_{\text{solv}}$.

To demonstrate the polarization of the nuclear density in a solvent environment, as well as to understand the effects of hydrogen bonding on the nuclear polarization, we examined the differences in proton density between the solvated and gas phases for the water dimer and four protonated water tetramer isomers. The NEO-DFT wave function ansatz is written

as a product of the electronic and nuclear Slater determinants $\Phi_e$ and $\Phi_p$:

$$\Psi_{\mathrm{NEO}}(\mathbf{x}^e, \mathbf{x}^p; \mathbf{r}^c) = \Phi_e(\mathbf{x}^e; \mathbf{r}^c)\Phi_p(\mathbf{x}^p; \mathbf{r}^c) \tag{1}$$

where $\mathbf{x}^e$ and $\mathbf{x}^p$ represent the electron and quantum proton collective spatial and spin coordinates, and $\mathbf{r}^c$ corresponds to the classical nuclear positions. As each proton is represented by a relatively localized proton orbital, the density for each proton can be computed as the square of the associated proton orbital. This localization allows protons to be treated in the analysis as distinguishable particles despite being fermions.

All calculations were conducted using a development version of ChronusQ[41] and validated against the same implementation in Q-Chem.[42] The PBE0 electronic functional[43] and the epc-17-2 electron-proton correlation functional[11] were used in the NEO calculations. The cc-pVTZ electronic basis set[44] and the PB4-D proton basis set[45] were used with a (99,590) integration grid. The calculations on the water dimers were performed on the optimized geometries of the water dimer in vacuum using CCSD(T)/CBS from the A24 dataset.[46] The calculations on the protonated water tetramers were performed on structures obtained from Ref. 47.

The proton density differences for the internal and external protons in the water dimer are plotted in Figure 1. Here, the proton polarization is depicted as a function of increasing solvent dielectric constant, from $\varepsilon = 2$, near the vacuum limit, to $\varepsilon = 100$, describing a highly polar solvent. The proton polarization is defined in this study as the density difference between the solvated and vacuum phase proton densities:

$$\Delta\rho_{\mathrm{proton}}(r) = \rho_{\mathrm{solv}}(r) - \rho_{\mathrm{vac}}(r). \tag{2}$$

The external proton in Figure 1(a-d) is observed to increasingly polarize in response to larger dielectric constant, starting with a smaller polarization at $\varepsilon = 2$ and developing a much more distinct effect by $\varepsilon = 100$. The internal proton, which is the hydrogen bond

donor, shows a similar response to solvation, where the proton polarization increases as a function of increasing dielectric, as shown in Figure 1(e-h). Within this explicitly hydrogen-bonded environment, the nuclear polarization is greater for the internal proton than that for the external proton, as indicated by a larger number of contours corresponding to a more significant change in density for the internal proton. Both the external and internal protons in this scheme experience solvent-induced nuclear polarization and intramolecular O-H bond polarization. It should be emphasized that the density of the internal proton is further modulated by additional polarization along the direction of the hydrogen bond. The nuclear density of the internal proton is therefore more delocalized than that of the external proton in vacuum, prior to any solvent polarization. This more delocalized proton density is more susceptible to polarization by the solvent, which results in the stronger polarization response for the internal proton compared to the external proton.

The nuclear polarization can also be described quantitatively by examining the equilibrium length of the O-H bond in solution and comparing against its length in vacuum. In both scenarios, the electronic and proton wave functions are fully optimized.[14,48] Here, the basis function centers for the quantum protons are fixed to the original classical positions, but the proton basis sets are large enough to allow proton polarization. The O-H bond length for a quantum proton is defined here as the distance between the oxygen nuclear position and the expectation value of the proton position operator:

$$r_{\mathrm{OH}} = |\mathbf{r}_{\mathrm{O}} - \langle\psi_p|\mathbf{r}|\psi_p\rangle| \tag{3}$$

where $\psi_p$ is the proton orbital for the single proton treated quantum mechanically. This change in bond length as a function of dielectric constant is shown in the corresponding panels in Figure 1 alongside the proton density differences. Solvation is found to slightly increase the O-H bond length for both the external and hydrogen-bonded protons, and the bond elongation increases with increasing value of $\varepsilon$, consistent with the nuclear polarization.

Smaller values of $\varepsilon = 2$ produce an increase of $1.6 \times 10^{-3}$ Bohr, whereas larger values of $\varepsilon = 100$ increase the bond length by $4.5 \times 10^{-3}$ Bohr for the external proton. The bond length of the internal O-H bond is larger than its external counterpart with bond length increases of $3.1 \times 10^{-3}$ Bohr at $\varepsilon = 2$ and $7.1 \times 10^{-3}$ Bohr at $\varepsilon = 100$, in agreement with the difference in polarization magnitude between the external and internal protons. Finally, it is important to note that the polarization response of the nuclear density is not linear with respect to the dielectric constant. The largest change in O-H bond length occurs between $\varepsilon = 2$ and $\varepsilon = 25$. For $\varepsilon > 25$, the O-H bond length slowly approaches the asymptotic limit of solvent polarization. This behavior is exemplified by the solvation free energies in Figure 1, which begin to converge past $\varepsilon = 25$ for both systems.

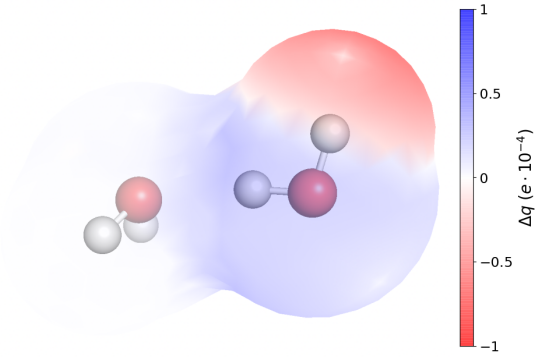


**Figure 2.** Difference in the apparent surface charges on the molecular cavity between a NEO and a conventional converged IEF-PCM calculation on the water dimer with only the external proton on the right treated quantum mechanically and with a dielectric constant of $\varepsilon = 78.35$. The continuous cavity surface shown here is a visual aid to represent the actual discretized surface made up of apparent surface charges. Here red indicates a decrease in surface charges and blue indicates an increase in surface charges upon proton quantization.

While the previous analysis examined the polarization of the nuclear density in a solvent environment compared to vacuum, the following analysis seeks to elucidate how the solvent is polarized within the NEO framework compared to the conventional framework in which all protons are treated classically as point charges. For the case of the external proton treated quantum mechanically, Figure 2 plots the difference in apparent surface charges on the cavity at a dielectric constant of $\varepsilon = 78.35$, corresponding to water at ambient conditions. This

quantity is calculated as

$$\Delta Q_{\text{surface}} = Q_{\text{surface}}^{\text{NEO}} - Q_{\text{surface}}^{\text{Classical}} \tag{4}$$

which quantitatively compares the surface charges representing the solvent polarization from a conventional PCM calculation with all nuclei treated classically against its NEO analog with an external proton treated quantum mechanically. Here, the surface charges around the oxygen gain net positive charge, whereas the surface charges around the external hydrogen gain net negative charge when the external proton is treated quantum mechanically within the NEO approach, leading to a broad increase in cavity surface polarization. In other words, within the NEO-PCM framework, negative surface charges become more negative and positive surface charges become more positive. This behavior is a result of the mutual polarization of the quantum proton and the solvent, which is absent when the proton is treated classically as a point charge. Furthermore, within these calculations, the surface polarization due to the NEO approach is localized to the surface near the quantum proton and its adjacent oxygen, suggesting that proton quantization does not influence the more distant regions of the solvent. This observation also implies that the changes in solvent polarization due to proton quantization do not significantly affect the more distant components of the solute.

Moving toward a more complete overview of nuclear polarization in solution, the final set of results in this work examines the proton polarization of protonated water tetramers, where all nine protons are treated quantum mechanically. Figure 3 displays the polarization of the proton density for four protonated water tetramers for $\varepsilon$ values of 2, 10, and 100. The proton polarization increases with increasing $\varepsilon$, in line with the previous polarization analyses on the water dimer in Figure 1. It is interesting to note that many of the protons polarize in a vertical direction relative to the molecular plane, with this phenomenon being particularly evident for protons in the hydronium and central $H_2O$-$H_3O$ heterodimer within these clusters. Also notable is that the internal protons, especially on the hydronium in the ring tetramer, displayed in panels Figure 3(d-f), polarize at slightly different angles depending

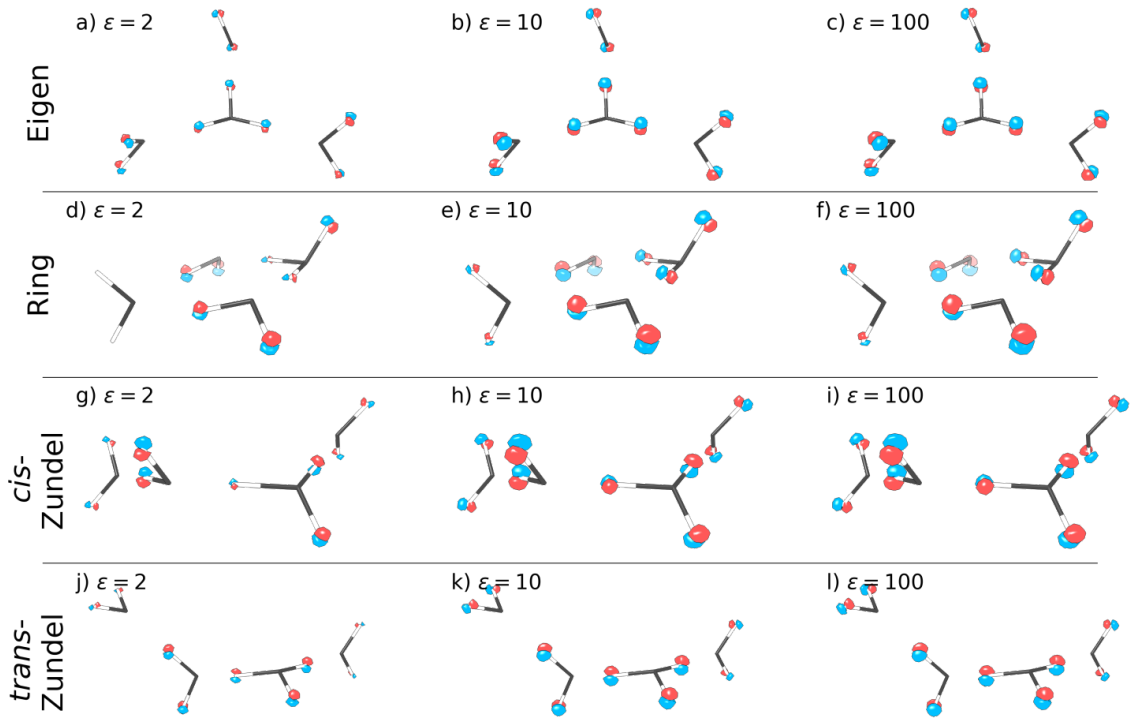


**Figure 3.** Polarization of the proton density between solvated and gas-phase calculations for four different protonated water tetramer isomers in dielectric environments of $\varepsilon = 2 - 100$. The classical hydrogen positions are drawn in white as a guide to the eye, and the oxygen atoms are drawn in grey. The red and blue isosurfaces correspond to $\Delta\rho$ values of $-0.1$ and 0.1 a.u., respectively.

on the dielectric constant. At $\varepsilon = 2$, the polarization is within the central plane, whereas at $\varepsilon = 10$ and $\varepsilon = 100$, the protons polarize in an out-of-plane direction. This is a consequence of the competition between proton polarization due to intramolecular interactions and proton polarization due to the solvent as the dielectric constant changes.

This Letter highlights the modulation of nuclear polarization by the solvent environment and the importance of using a quantum proton description in polarizable conditions. Our calculations show that increasing solvent polarity results in greater proton density polarization and longer O-H bond lengths. The subtle differences in nuclear polarization and OH bond elongation between the external and hydrogen-bonded protons can be resolved in the NEO-PCM approach. Moreover, the mutual polarization between the quantum protons and the solvent leads to greater solvent polarization for calculations with quantized protons than for calculations with protons treated classically as point charges. These effects on proton

polarization and solvent response will be especially important for studying proton chemical reactivity in processes such as proton transfer and proton-coupled electron transfer.

## Acknowledgements

The studies of the effect of solvated environment is supported by IDREAM (Interfacial Dynamics in Radioactive Environments and Materials), an Energy Frontier Research Center funded by the U.S. Department of Energy (DOE), Office of Science, Basic Energy Sciences (BES). The development of solvated nuclear-electronic orbital theory methods is supported by the Department of Energy in the Computational Chemical Science program (Grant No. DE-SC0023284). The development of the Chronus Quantum computational software is supported by the Office of Advanced Cyberinfrastructure, National Science Foundation (Grant No. OAC-2103717). All figures in this paper were generated using Matplotlib.[49] Molecular graphics were visualized using UCSF Chimera[50] and PyMol.[51]

## References

(1) Weinberg, D. R.; Gagliardi, C. J.; Hull, J. F.; Murphy, C. F.; Kent, C. A.; Westlake, B. C.; Paul, A.; Ess, D. H.; McCafferty, D. G.; Meyer, T. J. Proton-Coupled Electron Transfer. *Chem. Rev.* **2012**, *112*, 4016–4093.

(2) Pavošević, F.; Culpitt, T.; Hammes-Schiffer, S. Multicomponent Quantum Chemistry: Integrating Electronic and Nuclear Quantum Effects via the Nuclear–Electronic Orbital Method. *Chem. Rev.* **2020**, *120*, 4222–4253.

(3) Jankowska, J.; Sobolewski, A. L. Modern Theoretical Approaches to Modeling the Excited-State Intramolecular Proton Transfer: An Overview. *Molecules* **2021**, *26*, 5140.

(4) Webb, S. P.; Iordanov, T.; Hammes-Schiffer, S. Multiconfigurational Nuclear-Electronic

Orbital Approach: Incorporation of Nuclear Quantum Effects in Electronic Structure Calculations. *J. Chem. Phys.* **2002**, *117*, 4106–4118.

(5) Zhao, L.; Tao, Z.; Pavošević, F.; Wildman, A.; Hammes-Schiffer, S.; Li, X. Real-Time Time-Dependent Nuclear-Electronic Orbital Approach: Dynamics Beyond the Born-Oppenheimer Approximation. *J. Phys. Chem. Lett.* **2020**, *11*, 4052–4058.

(6) Zhao, L.; Wildman, A.; Tao, Z.; Schneider, P.; Hammes-Schiffer, S.; Li, X. Nuclear–Electronic Orbital Ehrenfest Dynamics. *J. Chem. Phys.* **2020**, *153*, 224111.

(7) Zhao, L.; Wildman, A.; Pavošević, F.; Tully, J. C.; Hammes-Schiffer, S.; Li, X. Excited State Intramolecular Proton Transfer with Nuclear-Electronic Orbital Ehrenfest Dynamics. *J. Phys. Chem. Lett.* **2021**, *12*, 3497–3502.

(8) Tao, Z.; Yu, Q.; Roy, S.; Hammes-Schiffer, S. Direct Dynamics With Nuclear–Electronic Orbital Density Functional Theory. *Acc. Chem. Res.* **2021**, *54*, 4131–4141.

(9) Pak, M. V.; Chakraborty, A.; Hammes-Schiffer, S. Density Functional Theory Treatment of Electron Correlation in the Nuclear- Electronic Orbital Approach. *J. Phys. Chem. A* **2007**, *111*, 4522–4526.

(10) Yang, Y.; Brorsen, K. R.; Culpitt, T.; Pak, M. V.; Hammes-Schiffer, S. Development of a Practical Multicomponent Density Functional for Electron-Proton Correlation to Produce Accurate Proton Densities. *J. Chem. Phys.* **2017**, *147*, 114113.

(11) Brorsen, K. R.; Yang, Y.; Hammes-Schiffer, S. Multicomponent Density Functional Theory: Impact of Nuclear Quantum Effects on Proton Affinities and Geometries. *J. Phys. Chem. Lett.* **2017**, *8*, 3488–3493.

(12) Pavošević, F.; Culpitt, T.; Hammes-Schiffer, S. Multicomponent Coupled Cluster Singles and Doubles Theory Within the Nuclear-Electronic Orbital Framework. *J. Chem. Theory Comput.* **2018**, *15*, 338–347.

(13) Swalina, C.; Pak, M. V.; Hammes-Schiffer, S. Alternative Formulation of Many-Body Perturbation Theory for Electron–Proton Correlation. *Chem. Phys. Lett.* **2005**, *404*, 394–399.

(14) Wildman, A.; Tao, Z.; Zhao, L.; Hammes-Schiffer, S.; Li, X. Solvated Nuclear–Electronic Orbital Structure and Dynamics. *J. Chem. Theory Comput.* **2022**, *18*, 1340–1346.

(15) Kanematsu, Y.; Tachikawa, M. Development of Multicomponent Hybrid Density Functional Theory With Polarizable Continuum Model for the Analysis of Nuclear Quantum Effect and Solvent Effect on NMR Chemical Shift. *J. Chem. Phys.* **2014**, *140*, 164111.

(16) Kanematsu, Y.; Tachikawa, M. Performance Test of Multicomponent Quantum Mechanical Calculation With Polarizable Continuum Model for Proton Chemical Shift. *J. Phys. Chem. A* **2015**, *119*, 4933–4938.

(17) Miertuš, S.; Scrocco, E.; Tomasi, J. Electrostatic Interaction of a Solute With a Continuum. A Direct Utilizaion of AB Initio Molecular Potentials for the Prevision of Solvent Effects. *Chem. Phys.* **1981**, *55*, 117–129.

(18) Mennucci, B. Polarizable Continuum Model. *WIREs Comput. Mol. Sci.* **2012**, *2*, 386–404.

(19) Herbert, J. M. Dielectric Continuum Methods for Quantum Chemistry. *WIREs Comput. Mol. Sci.* **2021**, *11*, e1519.

(20) Amovilli, C.; Barone, V.; Cammi, R.; Cancès, E.; Cossi, M.; Mennucci, B.; Pomelli, C. S.; Tomasi, J. Recent Advances in the Description of Solvent Effects With the Polarizable Continuum Model. *Adv. Quantum Chem.* **1998**, *32*, 227–261.

(21) Tomasi, J.; Cammi, R.; Mennucci, B. Medium Effects on the Properties of Chemical

Systems: An Overview of Recent Formulations in the Polarizable Continuum Model (PCM). *Int. J. Quant. Chem.* **1999**, *75*, 783–803.

(22) Cammi, R.; Mennucci, B.; Tomasi, J. Computational Modelling of the Solvent Effects on Molecular Properties: An Overview of the Polarizable Continuum Model (PCM) Approach. *Comput. Chem. Rev. Curr. Trends* **2003**, 1–79.

(23) Tomasi, J.; Mennucci, B.; Cammi, R. Quantum Mechanical Continuum Solvation Models. *Chem. Rev.* **2005**, *105*, 2999–3094.

(24) Mennucci, B.; Cammi, R. *Continuum Solvation Models in Chemical Physics: From Theory to Applications*; John Wiley & Sons: West Sussex, 2008.

(25) Lipparini, F.; Mennucci, B. Perspective: Polarizable Continuum Models for Quantum-Mechanical Descriptions. *J. Chem. Phys.* **2016**, *144*, 160901.

(26) Barone, V.; Cossi, M. Quantum Calculation of Molecular Energies and Energy Gradients in Solution by a Conductor Solvent Model. *J. Phys. Chem. A* **1998**, *102*, 1995–2001.

(27) Cossi, M.; Rega, N.; Scalmani, G.; Barone, V. Energies Structures and Electronic Properties of Molecules in Solution With the C-PCM Solvation Model. *J. Comput. Chem.* **2003**, *24*, 669–681.

(28) Klamt, A.; Schüürmann, G. COSMO: A New Approach to Dielectric Screening in Solvents With Explicit Expressions for the Screening Energy and Its Gradient. *J. Chem. Soc. Perkin Trans.* **1993**, 799–805.

(29) Lipparini, F.; Stamm, B.; Cances, E.; Maday, Y.; Mennucci, B. Fast Domain Decomposition Algorithm for Continuum Solvation Models: Energy and First Derivatives. *J. Chem. Theory Comput.* **2013**, *9*, 3637–3648.

(30) Lipparini, F.; Scalmani, G.; Lagardère, L.; Stamm, B.; Cancès, E.; Maday, Y.; Piquemal, J.-P.; Frisch, M. J.; Mennucci, B. Quantum Classical and Hybrid QM/MM Calculations in Solution: General Implementation of the ddCOSMO Linear Scaling Strategy. *J. Chem. Phys.* **2014**, *141*, 184108.

(31) Stamm, B.; Lagardère, L.; Scalmani, G.; Gatto, P.; Cancès, E.; Piquemal, J.-P.; Maday, Y.; Mennucci, B.; Lipparini, F. How to Make Continuum Solvation Incredibly Fast in a Few Simple Steps: A Practical Guide to the Domain Decomposition Paradigm for the Conductor-Like Screening Model. *Int. J. Quant. Chem.* **2019**, *119*, e25669.

(32) Cances, E.; Mennucci, B.; Tomasi, J. a New Integral Equation Formalism for the Polarizable Continuum Model: Theoretical Background and Applications to Isotropic and Anisotropic Dielectrics. *J. Chem. Phys.* **1997**, *107*, 3032–3041.

(33) Mennucci, B.; Cances, E.; Tomasi, J. Evaluation of Solvent Effects in Isotropic and Anisotropic Dielectrics and in Ionic Solutions With a Unified Integral Equation Method: Theoretical Bases Computational Implementation and Numerical Applications. *J. Phys. Chem. B* **1997**, *101*, 10506–10517.

(34) Cancès, E.; Mennucci, B. New Applications of Integral Equations Methods for Solvation Continuum Models: Ionic Solutions and Liquid Crystals. *J. Math. Chem.* **1998**, *23*, 309–326.

(35) Chipman, D. M. Simulation of Volume Polarization in Reaction Field Theory. *J. Chem. Phys.* **1999**, *110*, 8012–8018.

(36) Chipman, D. M. New Formulation and Implementation for Volume Polarization in Dielectric Continuum Theory. *J. Chem. Phys.* **2006**, *124*, 224111.

(37) Lange, A. W.; Herbert, J. M. Improving Generalized Born Models by Exploiting Connections to Polarizable Continuum Models. I. An Improved Effective Coulomb Operator. *J. Chem. Theory Comput.* **2012**, *8*, 1999–2011.

(38) Lange, A. W.; Herbert, J. M. Improving Generalized Born Models by Exploiting Connections to Polarizable Continuum Models. II. Corrections for Salt Effects. *J. Chem. Theory Comput.* **2012**, *8*, 4381–4392.

(39) Klamt, A.; Jonas, V. Treatment of the Outlying Charge in Continuum Solvation Models. *J. Chem. Phys.* **1996**, *105*, 9972–9981.

(40) Cossi, M.; Barone, V. Solvent Effect on Vertical Electronic Transitions by the Polarizable Continuum Model. *J. Chem. Phys.* **2000**, *112*, 2427–2435.

(41) Williams-Young, D. B.; Petrone, A.; Sun, S.; Stetina, T. F.; Lestrange, P.; Hoyer, C. E.; Nascimento, D. R.; Koulias, L.; Wildman, A.; Kasper, J.; Goings, J. J.; Ding, F.; DePrince III, A. E.; Valeev, E. F.; Li, X. The Chronus Quantum (ChronusQ) Software Package. *WIREs Comput. Mol. Sci.* **2019**, e1436.

(42) Epifanovsky, E.; Gilbert, A. T.; Feng, X.; Lee, J.; Mao, Y.; Mardirossian, N.; Pokhilko, P.; White, A. F.; Coons, M. P.; Dempwolff, A. L., et al. Software for the Frontiers of Quantum Chemistry: An Overview of Developments in the Q-Chem 5 Package. *J. Chem. Phys.* **2021**, *155*, 084801.

(43) Adamo, C.; Barone, V. Toward Reliable Density Functional Methods Without Adjustable Parameters: The PBE0 Model. *J. Chem. Phys.* **1999**, *110*, 6158–6170.

(44) Dunning Jr, T. H. Gaussian Basis Sets for Use in Correlated Molecular Calculations. I. The Atoms Boron Through Neon and Hydrogen. *J. Chem. Phys.* **1989**, *90*, 1007–1023.

(45) Yu, Q.; Pavošević, F.; Hammes-Schiffer, S. Development of Nuclear Basis Sets for Multicomponent Quantum Chemistry Methods. *J. Chem. Phys.* **2020**, *152*, 244123.

(46) Rezac, J.; Hobza, P. Describing Noncovalent Interactions Beyond the Common Approximations: How Accurate Is the "Gold Standard" CCSD (T) at the Complete Basis Set Limit? *J. Chem. Theory Comput.* **2013**, *9*, 2151–2155.

(47) Heindel, J. P.; Yu, Q.; Bowman, J. M.; Xantheas, S. S. Benchmark Electronic Structure Calculations for H3O+ (H2O) N N. *J. Chem. Theory Comput.* **2018**, *14*, 4553–4566.

(48) Liu, A.; Chow, M.; Wildman, A.; Frisch, M. J.; Hammes-Schiffer, S.; Li, X. Simultaneous Optimization of Nuclear–Electronic Orbitals. *J. Phys. Chem. A* **2022**, *126*, 7033–7039.

(49) Hunter, J. D. Matplotlib: A 2D Graphics Environment. *Comput. Sci. Eng.* **2007**, *9*, 90–95.

(50) Pettersen, E. F.; Goddard, T. D.; Huang, C. C.; Couch, G. S.; Greenblatt, D. M.; Meng, E. C.; Ferrin, T. E. UCSF Chimera—A Visualization System for Exploratory Research and Analysis. *J. Comput. Chem.* **2004**, *25*, 1605–1612.

(51) Schrödinger, LLC, The PyMOL Molecular Graphics System Version 1.8. 2015.